Electronic Supplementary Material (ESI) for Catalysis Science & Technology.
This journal is © The Royal Society of Chemistry 2022

Electronic Supplementary Information

Nitrile hydrogenation to secondary amines under ambient conditions over palladium-platinum random alloy nanoparticles

Yoshihide Nishida *[a,1], Katsutoshi Sato *[a,b], Chandan Chaudhari [a,2], Hiroshi Yamada [a], Takaaki Toriyama [c], Tomokazu Yamamoto [d], Syo Matsumura [c,d], Susan Meñez Aspera [e], Hiroshi Nakanishi [e], Masaaki Haneda [f,g] and Katsutoshi Nagaoka *[a]

[a] *Department of Chemical Systems Engineering, Graduate School of Engineering, Nagoya University, Furo-cho, Chikusa-ku, Nagoya 464-8603, Japan*

[b] *Elements Strategy Initiative for Catalysts and Batteries, Kyoto University, 1-30 Goryo-Ohara, Nishikyo-ku, Kyoto 615-8245, Japan*

[c] *The Ultramicroscopy Research Center, Kyushu University, 744 Motooka, Nishi-ku, Fukuoka 819-0395, Japan*

[d] *Department of Applied Quantum Physics and Nuclear Engineering, Kyushu University, 744 Motooka, Nishi-ku, Fukuoka 819-0395, Japan*

[e] *National Institute of Technology, Akashi College, 679-3 Nishioka, Uozumi, Akashi, Hyogo 674-8501, Japan*

[f] *Advanced Ceramics Research Center, Nagoya Institute of Technology, 10-6-29 Asahigaoka, Tajimi, Gifu 507-0071, Japan*

[g] *Frontier Research Institute for Materials Science, Nagoya Institute of Technology, Gokiso-cho, Showa-ku, Nagoya 466-8555, Japan*

[1] *(Present address) Advanced Ceramics Research Center, Nagoya Institute of Technology, 10-6-29 Asahigaoka, Tajimi, Gifu 507-0071, Japan*

[2] *(Present address) Renewable Energy Research Center, National Institute of Advanced Industrial Science and Technology, 2-2-9 Machiikedai, Koriyama, Fukushima 963-0298, Japan*

1. Methods

Transmission Electron Microscopy

The morphologies of the PVP-stabilized metal nanoparticles were determined from transmission electron microscopy (TEM) images recorded with a JEM-2100 Plus microscope (JEOL, Japan) operated at an accelerating voltage of 200 kV.

Thermogravimetric Analysis

The amount of PVP adsorbed on the metal nanoparticles and the metal loading of carbon-supported catalysts were determined by means of thermogravimetric analysis (TGA) with a ThermoPlus instrument (Rigaku, Japan). Samples were heated from 25 to 1000 °C under air at a flow rate of 200 mL/min.

Scanning Transmission Electron Microscopy and Energy-Dispersive X-Ray Spectroscopy

The alloying state of the PdPt(50:50) nanoparticles was visualized by means of high-angle annular dark-field imaging and elemental maps based on Pd-L and Pt-L signals, which were obtained with a JEM-ARM200CF system (JEOL, Japan) operated at an accelerating voltage of 120 kV.

X-Ray Absorption Spectroscopy

The electronic states and local coordination structures of the PdPt-PVP nanoparticles were determined from X-ray absorption fine-structure spectra measured in transmittance mode at the BL01B1 beamline of the SPring-8 synchrotron radiation facility in Japan. Pd K- and Pt L_3-edge X-ray absorption fine-structure spectra were recorded at room temperature in air by using either a Si(311) or Si(111) monochromator. Data were analyzed by using the Athena software (ver. 0.9.26).

X-Ray Diffraction Analysis

The crystal structures of PdPt nanoparticles with different metal compositions were subjected to X-ray diffraction with a SmartLab X-ray diffractometer (Rigaku, Japan) with Cu Kα radiation.

Fourier Transform IR Spectroscopy

The surface states of the PdPt(50:50) nanoparticles were analyzed by means of Fourier transform IR spectroscopy with carbon monoxide (CO) as a probe molecule on an FT/IR-6600 instrument (JASCO, Japan) with a mercury-cadmium-telluride detector at a resolution of 4 cm^{-1}. SiO_2-supported metal nanoparticles were pressed into a pellet with a diameter of 10 mm, and the pellet was placed in a glass cell equipped with CaF_2 windows. The cell was connected to a gas-flow system, and the sample pellet was pretreated with flowing helium gas at 160 °C for 30 min. After the cell was cooled to 50 °C, 0.5% CO in helium was passed through the cell for 15 min, and then the cell was purged with flowing helium for 15 min. Then the IR spectrum was recorded at 50 °C.

Density Functional Theory Calculations

Density functional theory calculations were carried out with the Vienna ab initio simulation package.[1–4] The exchange–correlation term was described using a generalized gradient approximation based on the Perdew–Burke–Ernzerhof functional.[5–8] The interactions between ions and electrons were described by means of the projector augmented wave method.[9,10] Plane wave basis sets were employed with an energy cut-off of 500 eV. The slab model that was used had a 4 × 4 fcc (111) surface, five atomic layers, and an 18 Å thick vacuum space. The supercell for PdPt(50:50) random alloy nanoparticles contained 40 Pd atoms and 40 Pt atoms, and the elemental components were randomly mixed by means of a pseudorandom number generated by a computer. Electric dipole correction was used to cut the dipole interactions between the repeated image slabs. The surface Brillouin zone integrations were performed by means of the special-point sampling technique of Monkhorst and Pack with 3 × 3 × 1 sampling k-point meshes.[11] A conjugate-gradient algorithm[12] was used to relax the atomic positions in the upper three atomic layers into their ground states. The atomic positions of the two layers were fixed with the states of the bulk PdPt(50:50) random alloy.

2. Supplemental Figures and Tables

Table S1. Preparation of PVP-stabilized metal nanoparticles.

Catalyst	Precursor	Amount of precursor (mmol)	Particle size (nm)[a]	Amount of PVP (wt %)[b]
Ru-PVP	$RuCl_3 \cdot nH_2O$	0.250	3.2	81.8
Rh-PVP	$RhCl_3 \cdot 3H_2O$	0.250	5.0	82.0
Pd-PVP	$(NH_4)_2PdCl_4$	0.250	4.9	82.0
Ir-PVP	$(NH_4)_2IrCl_6$	0.250	1.8	78.7
Pt-PVP	$(NH_4)_2PtCl_4$	0.250	4.3	71.7
PdPt(50:50)-PVP	$(NH_4)_2PdCl_4$ $(NH_4)_2PtCl_4$	0.125 0.125	4.6	78.0

[a] Particle size was determined by counting 200 particles in the TEM images.

[b] The amount of PVP adsorbed on the metal was calculated by TGA.

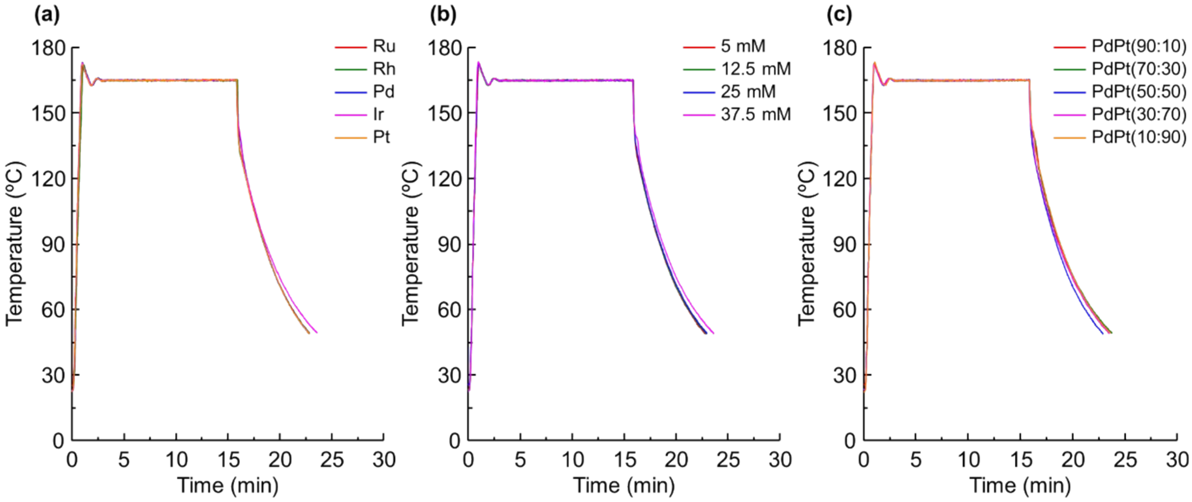

Figure S1. Time course of temperature during preparation of (a) monometallic nanoparticles, (b) PdPt(50:50) nanoparticles with different particle sizes, and (c) PdPt nanoparticles with different metal compositions.

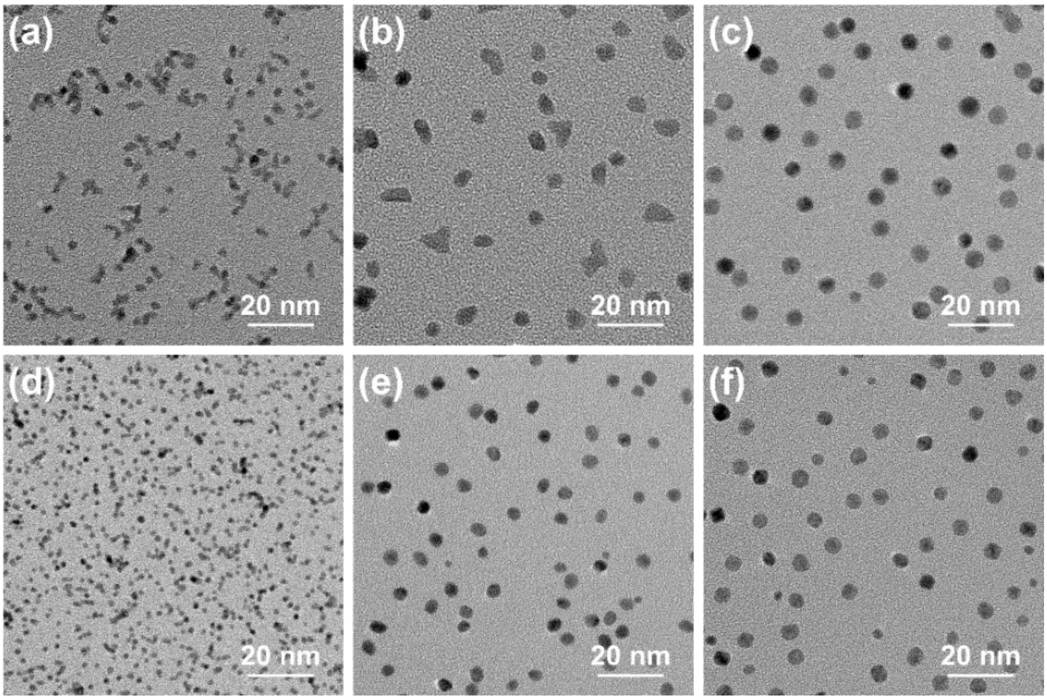

Figure S2. TEM images of (a) Ru, (b) Rh, (c) Pd, (d) Ir, (e) Pt, and (f) PdPt(50:50)-PVP nanoparticles prepared under the conditions listed in Table S1.

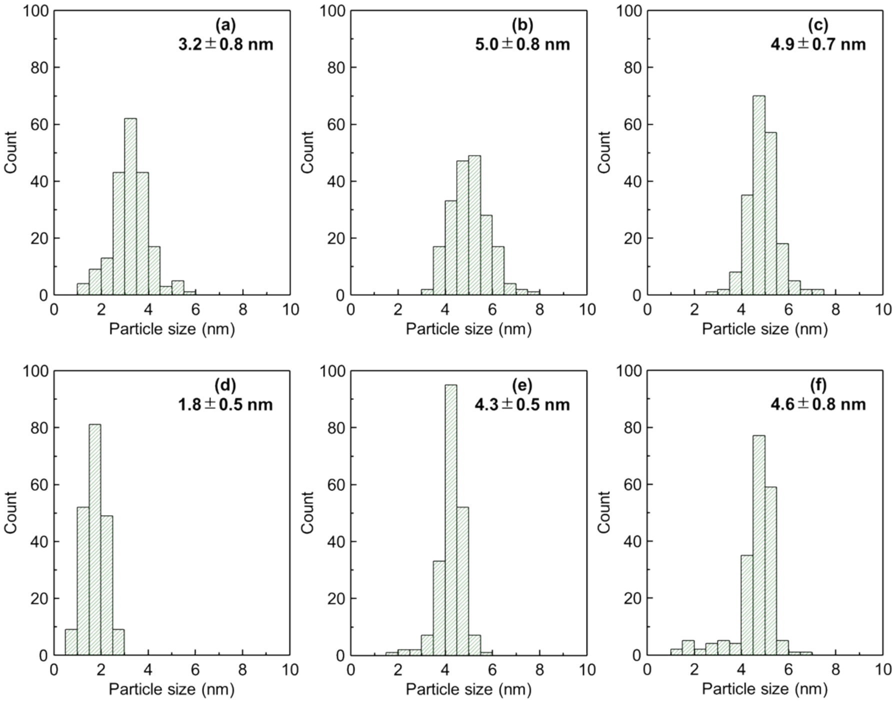

Figure S3. Particle-size distributions of (a) Ru, (b) Rh, (c) Pd, (d) Ir, (e) Pt, and (f) PdPt(50:50)-PVP nanoparticles prepared under the conditions listed in Table S1.

Table S2. Preparation of PdPt(50:50) nanoparticles of various sizes.

Particle size (nm)[a]	$(NH_4)_2PdCl_4$ (mmol)	$(NH_4)_2PtCl_4$ (mmol)	PVP (mmol)	EG (mL)	Metal concentration (mM)	Amount of PVP (wt %)[b]
3.9	0.050	0.050	0.50	20	5.0	77.3
4.6	0.125	0.125	1.25	20	12.5	78.0
6.8	0.250	0.250	2.50	20	25.0	79.8
8.4	0.375	0.375	3.75	20	37.5	79.4

[a] Particle size was determined by counting 200 particles in the TEM images.

[b] The amount of PVP adsorbed on the metal was calculated by TGA.

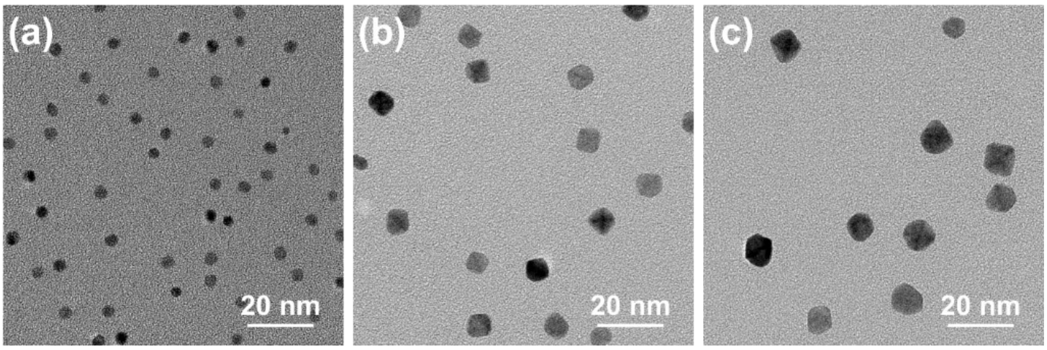

Figure S4. TEM images of PdPt(50:50) nanoparticles prepared using metal precursor concentrations of (a) 5.0, (b) 25.0, and (c) 37.5 mM. A TEM image of a sample prepared by using 12.5 mM metal precursors is shown in Figure S2f.

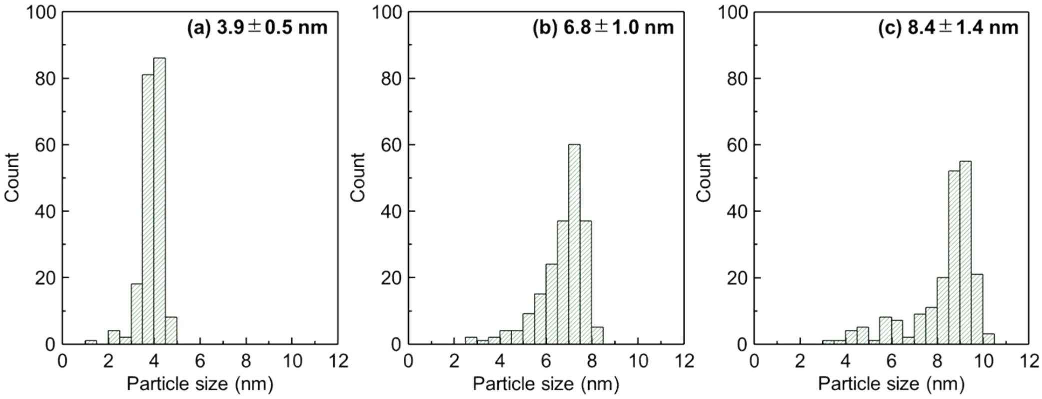

Figure S5. Particle-size distributions of PdPt(50:50) nanoparticles prepared using metal precursor concentrations of (a) 5.0, (b) 25.0, and (c) 37.5 mM. The particle-size distribution of a sample prepared by using 12.5 mM metal precursors is shown in Figure S3f.

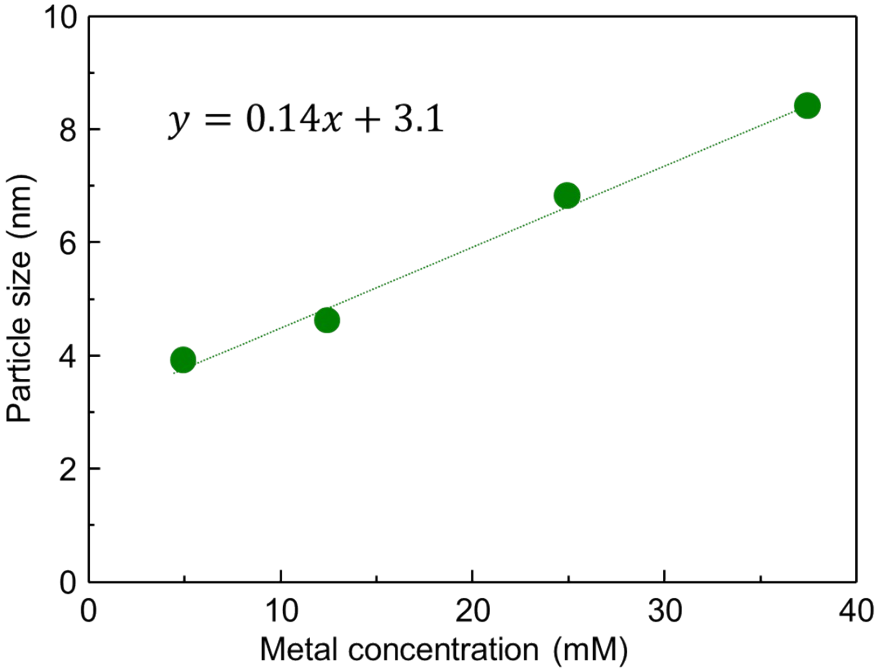

Figure S6. Metal-concentration dependence of size of PdPt(50:50) nanoparticles.

Table S3. Preparation of PdPt nanoparticles with various metal compositions.

	$(NH_4)_2PdCl_4$ (mmol)	$(NH_4)_2PtCl_4$ (mmol)	PVP (mmol)	EG (mL)	Particle size (nm)[a]	Amount of PVP (wt %)[b]
PdPt(90:10)	0.225	0.025	1.25	20	5.3	81.4
PdPt(70:30)	0.175	0.075	1.25	20	4.7	79.3
PdPt(50:50)	0.125	0.125	1.25	20	4.6	78.0
PdPt(30:70)	0.075	0.175	1.25	20	4.4	75.7
PdPt(10:90)	0.025	0.225	1.25	20	4.4	73.3

[a] Particle size was determined by counting 200 particles in the TEM images.

[b] The amount of PVP adsorbed on the metal was calculated by TGA.

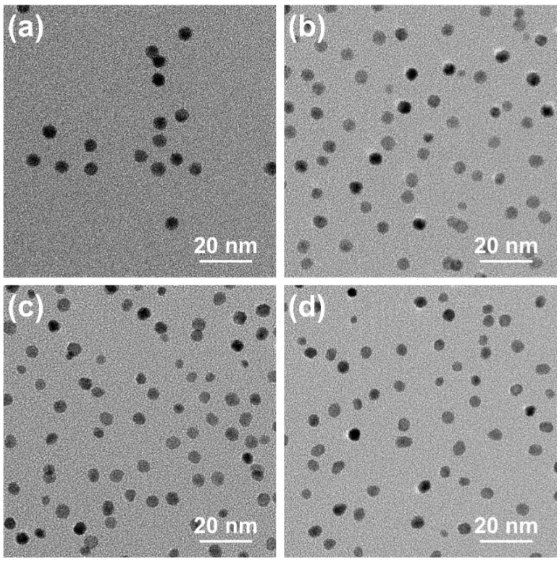

Figure S7. TEM images of (a) PdPt(90:10), (b) PdPt(70:30), (c) PdPt(30:70), and (d) PdPt(10:90) nanoparticles. A TEM image of PdPt(50:50) nanoparticles is shown in Figure S2f.

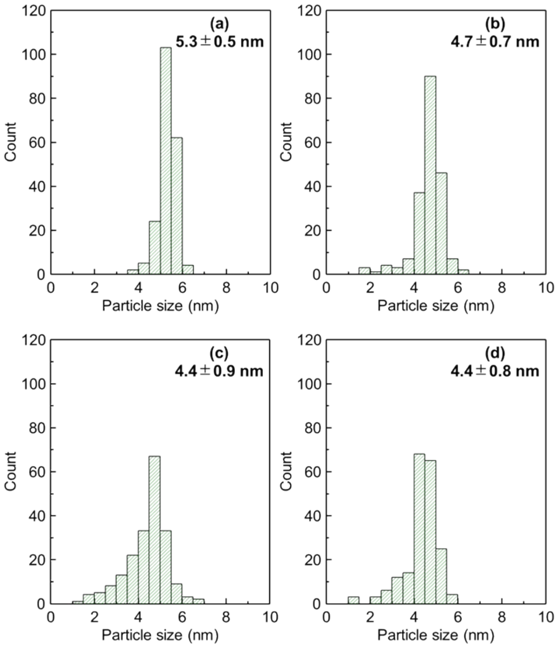

Figure S8. Particle-size distributions of (a) PdPt(90:10), (b) PdPt(70:30), (c) PdPt(30:70), and (d) PdPt(10:90) nanoparticles. The particle-size distribution of the PdPt(50:50) nanoparticles is shown in Figure S3f.

$$\text{Metal dispersion (\%)} = \frac{6 \times FW\ (\text{g/mol})}{6.02 \times \rho\ (\text{g/cm}^3) \times \sigma_m\ (\text{nm}^2) \times d\ (\text{nm})}$$

FW: Formula weight
ρ : Metal density
σ_m : Metal cross-sectional area
d : Particle size

Figure S9. Equation for estimating metal dispersion. The formula weight, metal density, and metal cross-sectional area of PdPt nanoparticles were calculated on the basis of the metal composition of the nanoparticles.

Table S4. Data related to the plots shown in Figure 1.

Catalyst	Conversion (%)[a]	Yield of 1° amine (%)[a]	Yield of 2° amine (%)[a]	Dispersion (%)[b]	TOF (h^{-1})[c]
Pd	12	9	1	23	20 (12)
PdPt(90:10)	33	27	5	21	75 (33)
PdPt(70:30)	43	7	32	24	81 (43)
PdPt(50:50)	60	0	55	25	129 (23)
PdPt(30:70)	47	0	41	26	80 (47)
PdPt(10:90)	18	0	13	26	25 (18)
Pt	13	0	9	26	17 (13)

[a] Conversion and yield were calculated by means of gas chromatography with flame ionization detection using dodecane as an internal standard.

[b] Metal dispersion was estimated according to the equation shown in Figure S9, on the assumption that the nanoparticles were spherical.

[c] Turnover frequency (TOF) was calculated from the metal dispersion and the total yield of benzene rings at bracketed conversions.

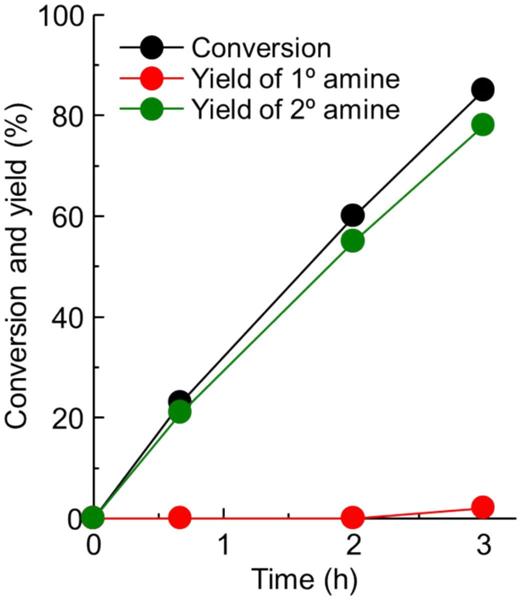

Figure S10. Time courses of substrate conversion and product yields during hydrogenation of benzonitrile over 4.6 nm PdPt(50:50) nanoparticles (reaction conditions are shown in Table 1).

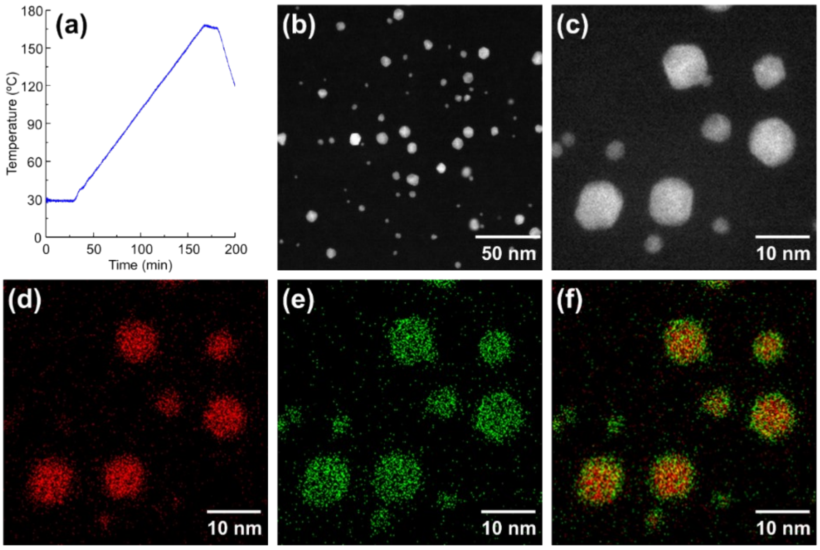

Figure S11. (a) Time course of temperature during preparation of PdPt(50:50) nanoparticles with a mantle heater. (b,c) High-angle annular dark-field images of the nanoparticles prepared with the mantle heater. (d) Pd-L and (e) Pt-L maps obtained by scanning transmission electron microscopy energy-dispersive X-ray spectroscopy analysis of the nanoparticles prepared with the mantle heater. (f) Overlay of the images in panels d and e.

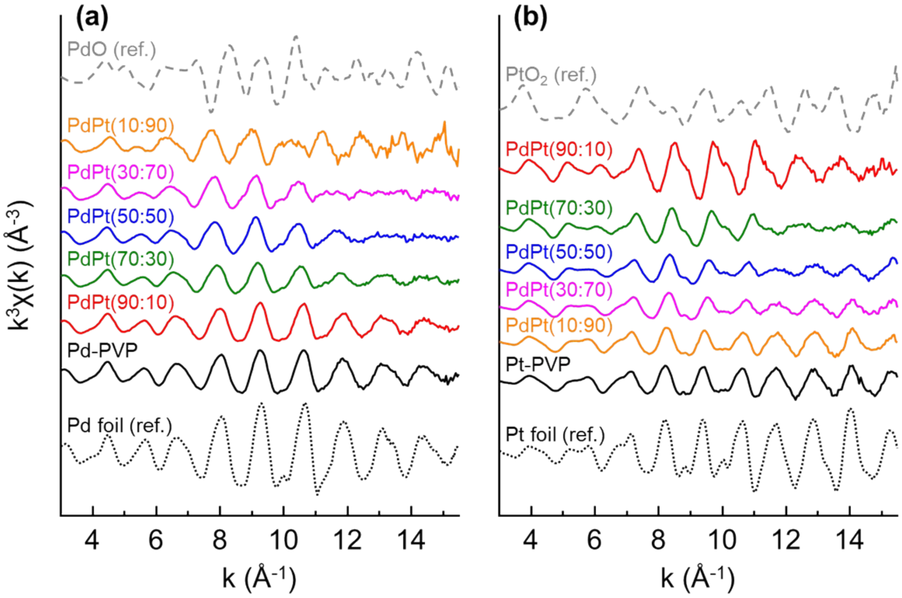

Figure S12. (a) Pd K-edge and (b) Pt L_3-edge extended X-ray absorption fine-structure oscillations of PdPt nanoparticles with various metal compositions.

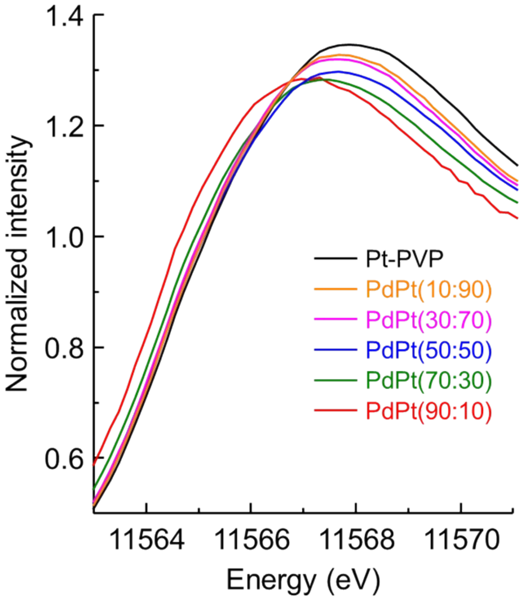

Figure S13. Detail of the Pt L_3-edge X-ray absorption near-edge structure spectra shown in Figure 2b.

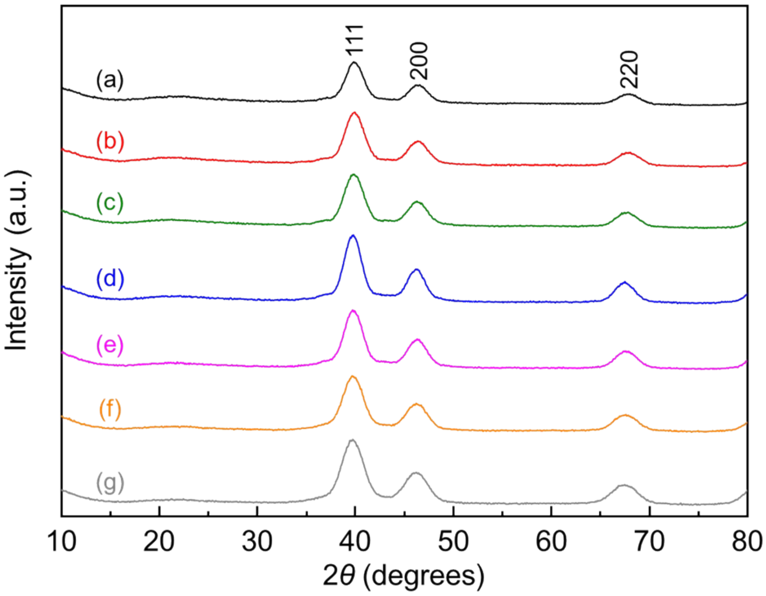

Figure S14. X-ray diffraction patterns of (a) Pd, (b) PdPt(90:10), (c) PdPt(70:30), (d) PdPt(50:50), (e) PdPt(30:70), (f) PdPt(10:90), and (g) Pt nanoparticles. The crystallite sizes calculated by means of the Scherrer equation were 4.3, 4.0, 3.9, 4.4, 4.1, 3.7, and 3.4 nm, respectively.

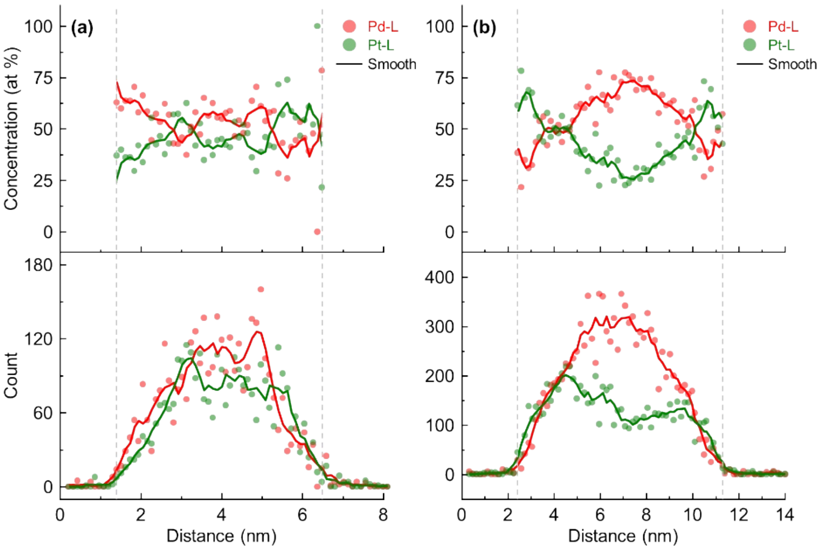

Figure S15. Line scan profiles for scanning transmission electron microscopy energy-dispersive X-ray spectroscopy analyses of (a) 3.9 and (b) 8.4 nm PdPt(50:50) nanoparticles.

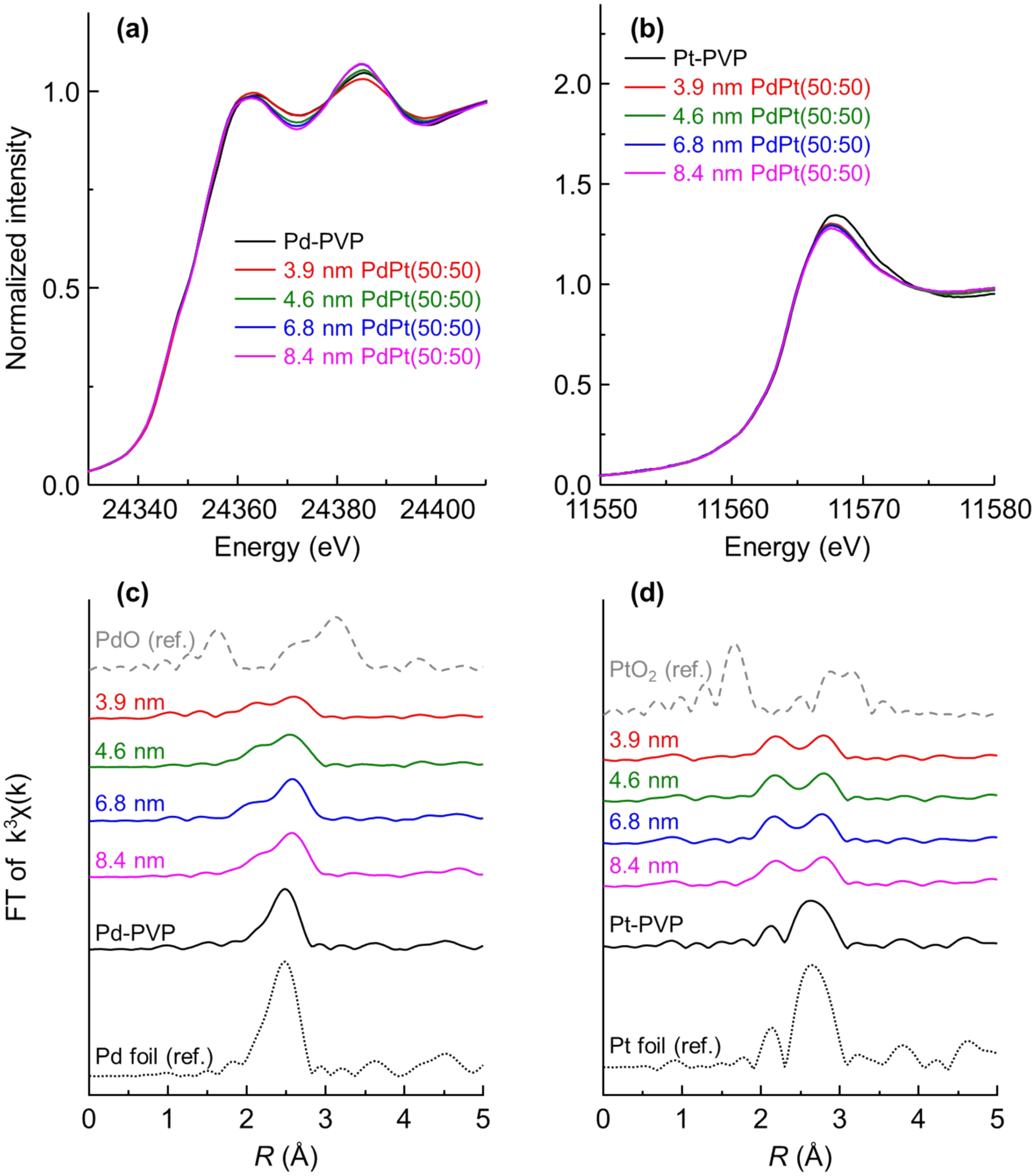

Figure S16. (a) Pd K-edge and (b) Pt L_3-edge X-ray absorption near-edge structure spectra of PdPt nanoparticles with various sizes. (c) Pd K-edge and (d) Pt L_3-edge FT extended X-ray absorption fine-structure spectra of PdPt nanoparticles with various sizes.

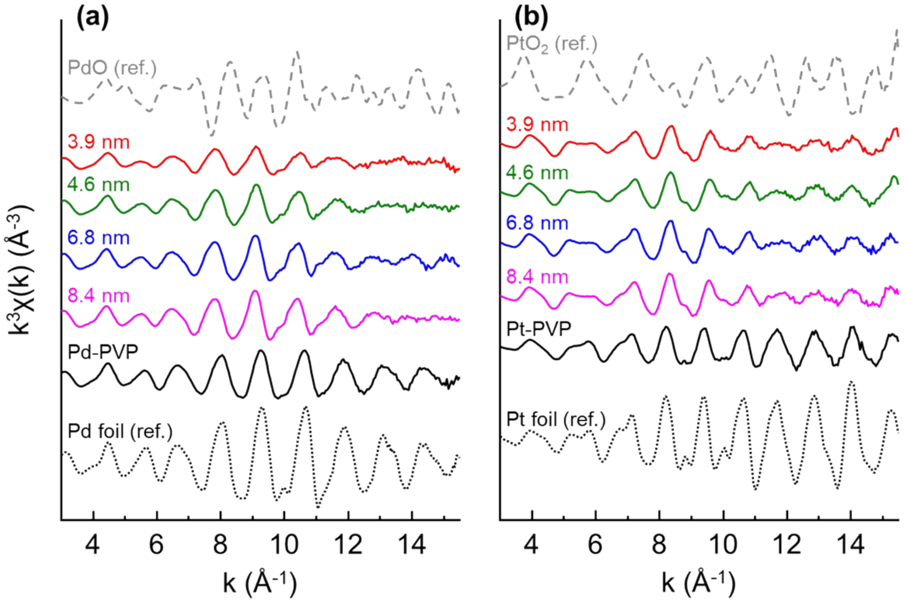

Figure S17. (a) Pd K-edge and (b) Pt L_3-edge extended X-ray absorption fine-structure oscillations of PdPt nanoparticles with various particle sizes.

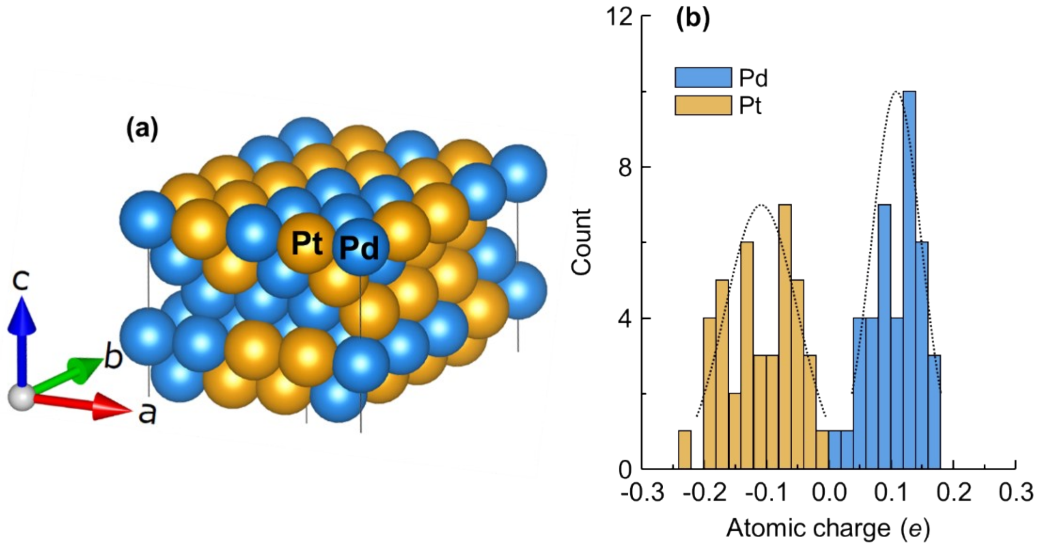

Figure S18. (a) Slab model of PdPt(50:50) random alloy nanoparticles and (b) the corresponding histogram of the atomic charges. The blue and yellow balls indicate Pd and Pt atoms, which were rendered using VESTA.[13] The atomic charges were obtained by means of Bader charge analysis.[14]

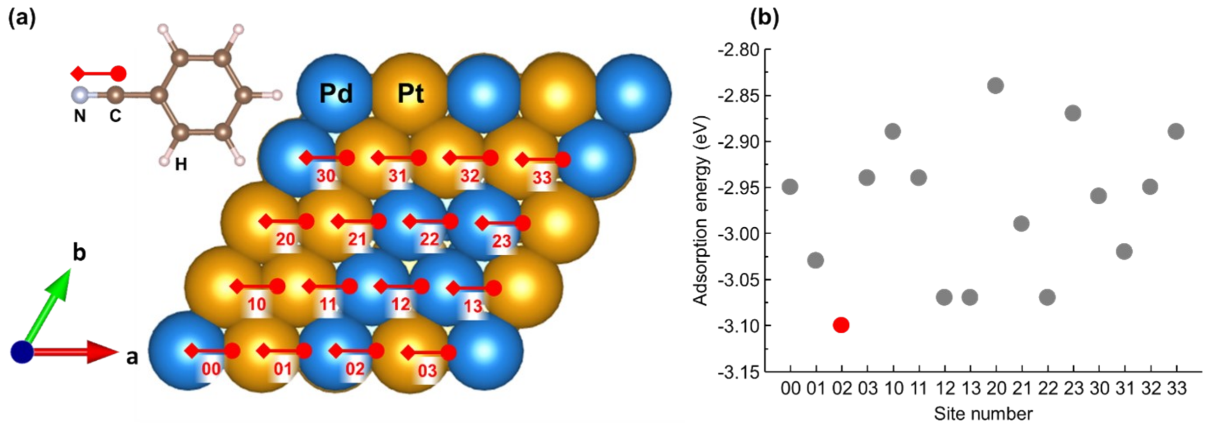

Figure S19. (a) Bridge sites for adsorption of benzonitrile on the 111 surface of PdPt(50:50) random alloy nanoparticles. (b) Corresponding energies for adsorption at each bridge site. In panel a, the positions of the nitrogen and carbon atoms of the cyano group are indicated by the connected red diamonds and circles, respectively. The blue and yellow balls indicate surface Pd and Pt atoms, which were rendered using VESTA.[13]

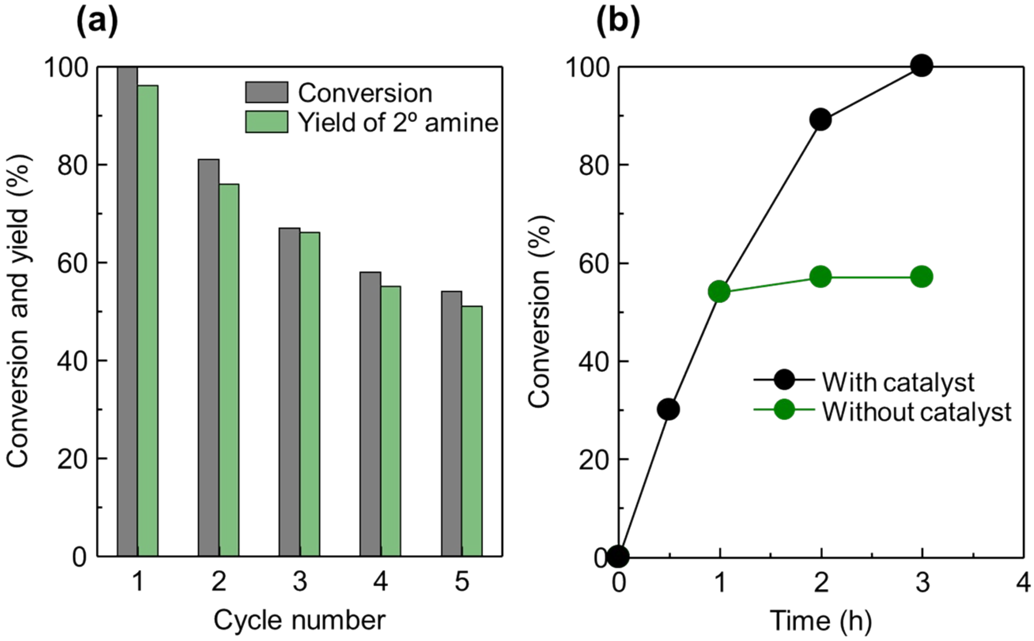

Figure S20. (a) Reuse and (b) leaching tests for benzonitrile hydrogenation catalyzed by carbon-supported 3.9 nm PdPt(50:50) nanoparticles under ambient conditions for 3 h.

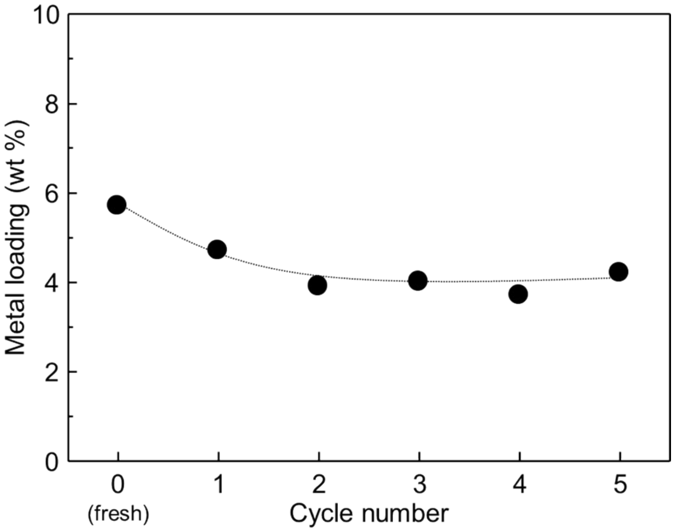

Figure S21. Metal loading of carbon-supported 3.9 nm PdPt(50:50) nanoparticles before and after the reaction.

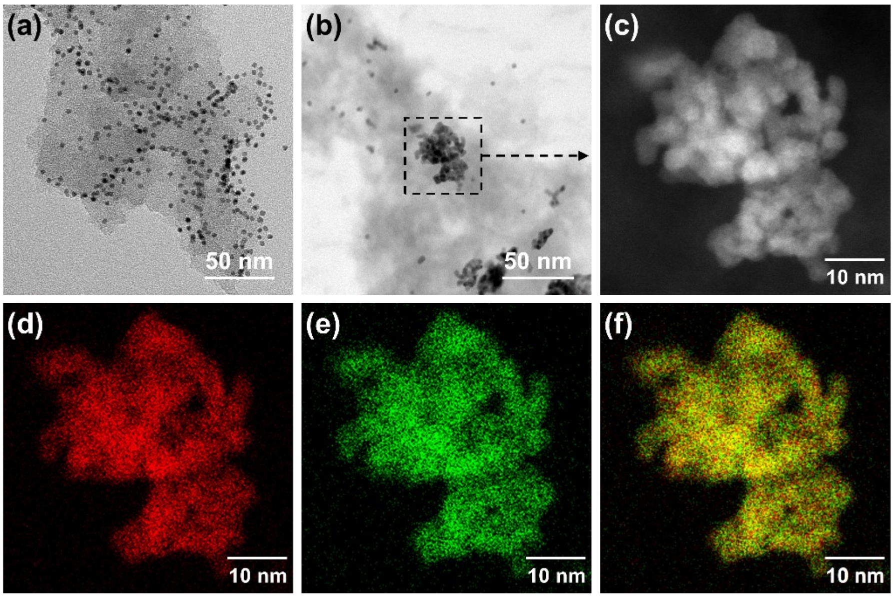

Figure S22. TEM and scanning transmission electron microscopy images of carbon-supported 3.9 nm PdPt(50:50) nanoparticles (a) before the hydrogenation reaction and (b) after five uses. (c) High-angle annular dark-field image of the nanoparticles after five uses. (d) Pd-L and (e) Pt-L maps obtained by scanning transmission electron microscopy energy-dispersive X-ray spectroscopy analysis of the nanoparticles after five uses. (f) Overlay of the images in panels d and e.

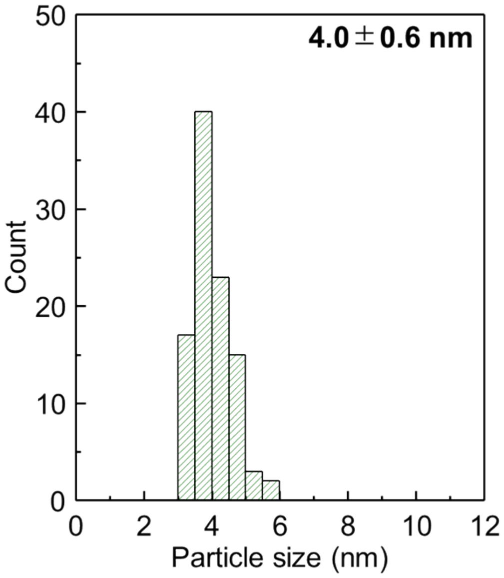

Figure S23. Particle-size distribution of carbon-supported 3.9 nm PdPt(50:50) nanoparticles after five uses.

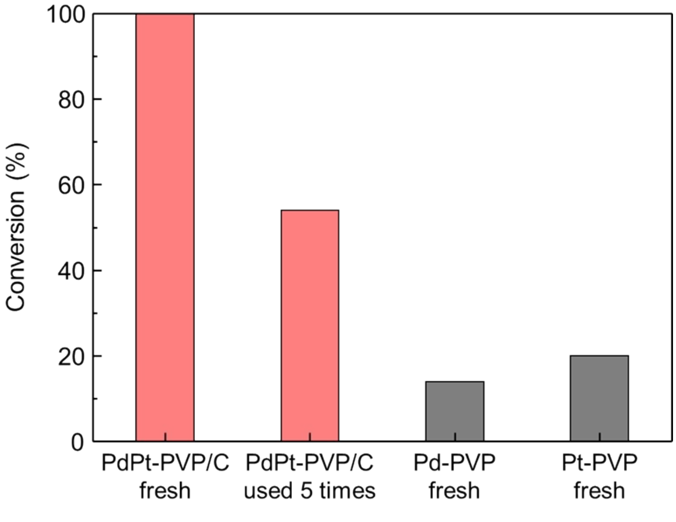

Figure S24. Comparison of the catalytic activities of fresh and reused nanoparticles for hydrogenation of benzonitrile under ambient conditions for 3 h.

Table S5. Comparison of the performance of the reported catalysts with our PdPt random alloy nanoparticle catalyst.

Entry	Catalyst (mol %)	Substrate	Temp. (°C)	H_2 (bar)	Time (h)	2°Amine yield (%)	Ref. in manuscript
1	PdPt(50:50)-PVP/C (Pd+Pt: 1)	Benzonitrile	25	1	3	96	**This study**
2	Re(I) complex (0.5)	Benzonitrile	140	75	1	90	17
3	Ru(II) complex (2)	Benzonitrile	80	60	12	90	18
4	Rh(I) complex (1)	Benzonitrile	60	10	21	81	19
5	Pd@mpg-C_3N_4 (0.2)	Benzonitrile	80	10	6	89	20
6	Pt nanowire (0.5)	Benzonitrile	80	1	24	95	21
7	Rh/Al_2O_3 (56)	Benzonitrile	25	1	20-30	85	22
8	Pd/C (5)	Cyclohexanecarbonitrile	25	1	24	93	23
9	Rh/C (5)	Cyclohexanecarbonitrile	25	1	24	92	23
10	PtMo nanowire (Pt+Mo: 0.5)	Benzonitrile	80	1	24	95	27
11	5Pd-Ni/SiO_2 (Pd+Ni: 2)	Benzonitrile	80	6	3	97	28
12	NiO-Pd/SiC (Ni+Pd: 1)	Benzonitrile	30	1	5	96	29

3. References

1 G. Kresse and J. Furthmüller, *Phys. Rev. B*, 1996, **54**, 11169-11186.

2 G. Kresse and J. Furthmüller, *Comput. Mater. Sci.*, 1996, **6**, 15-50.

3 G. Kresse and J. Hafner, *Phys. Rev. B*, 1993, **47**, 558-561.

4 G. Kresse and J. Hafner, *Phys. Rev. B*, 1994, **49**, 14251-14269.

5 J. P. Perdew, K. Burke and M. Ernzerhof, *Phys. Rev. Lett.*, 1996, **77**, 3865-3868.

6 J. P. Perdew, K. Burke and Y. Wang, *Phys. Rev. B*, 1996, **54**, 16533-16539.

7 A. D. Becke, *Phys. Rev. A*, 1988, **38**, 3098-3100.

8 C. Lee, W. Yang and R. G. Parr, *Phys. Rev. B*, 1988, **37**, 785-789.

9 P. E. Blochl, *Phys. Rev. B*, 1994, **50**, 17953-17979.

10 G. Kresse and D. Joubert, *Phys. Rev. B*, 1999, **59**, 1758-1775.

11 H. J. Monkhorst and J. D. Pack, *Phys. Rev. B*, 1976, **13**, 5188-5192.

12 I. I. Stich, R. Car, M. Parrinello and S. Baroni, *Phys. Rev. B*, 1989, **39**, 4997-5004.

13 K. Momma and F. Izumi, *J. Appl. Crystallogr.*, 2011, **44**, 1272-1276.

14 G. Henkelman, A. Arnaldsson and H. Jónsson, *Comput. Mater. Sci.*, 2006, **36**, 354-360.